Published in final edited form as:

Dev Cell. 2017 March 13; 40(5): 439–452.e4. doi:10.1016/j.devcel.2017.02.010.

A Wnt5 Activity Asymmetry and Intercellular Signaling via PCP Proteins Polarize Node Cells for Left-Right Symmetry Breaking

Katsura Minegishi[1,2,*], **Masakazu Hashimoto**[1], **Rieko Ajima**[1,3,12], **Katsuyoshi Takaoka**[1,13], **Kyosuke Shinohara**[1,14], **Yayoi Ikawa**[1,2], **Hiromi Nishimura**[1,2], **Andrew P. McMahon**[4], **Karl Willert**[5], **Yasushi Okada**[6], **Hiroshi Sasaki**[7], **Dongbo Shi**[8,15], **Toshihiko Fujimori**[8], **Toshihisa Ohtsuka**[9], **Yasunobu Igarashi**[10], **Terry P. Yamaguchi**[3], **Akihiko Shimono**[11,16], **Hidetaka Shiratori**[1,17], **Hiroshi Hamada**[1,2,18,*]

[1]Developmental Genetics Group, Graduate School of Frontier Biosciences, Osaka University, 1-3 Yamada-oka, Suita, Osaka 565-0871, Japan

[2]Laboratory for Organismal Patterning, RIKEN Center for Developmental Biology, 2-2-3 Minatojima-minamimachi, Chuo-ku, Kobe, Hyogo 650-0047, Japan

[3]Cancer and Developmental Biology Laboratory, Center for Cancer Research, National Cancer Institute-Frederick, NIH, Frederick, MD 21702, USA

[4]Department of Stem Cell Biology and Regenerative Medicine, Keck School of Medicine of the University of Southern California, Los Angeles, CA 90033, USA

[5]Department of Cellular and Molecular Medicine, University of California San Diego, La Jolla, CA 92093, USA

[6]Laboratory for Cell Polarity Regulation, RIKEN Quantitative Biology Center, 6-2-3 Furuedai, Suita, Osaka 565-0874, Japan

[7]Laboratory for Embryogenesis, Graduate School of Frontier Biosciences, Osaka University, 1-3 Yamada-oka, Suita, Osaka 565-0871, Japan

[8]Division of Embryology, National Institute for Basic Biology, 5-1 Higashiyama, Myodaiji, Okazaki, Aichi 444-8787, Japan

[9]Department of Biochemistry, Faculty of Medicine/Graduate School of Medicine, University of Yamanashi, 1110 Shimo-Kato, Chuo, Yamanashi 409–3898, Japan

[*]Correspondence: hiroshi.hamada@riken.jp (H.H.), katsura.minegishi@riken.jp (K.M.).

AUTHOR CONTRIBUTIONS

K.M. designed, performed, and analyzed most of the experiments. K.S. performed particle image velocimetry analysis. M.H. contributed to the initial phase of this work. R.A., K.T., and H. Shiratori designed and analyzed some of the experiments such as those involving chimera embryos. Y. Ikawa, H.N., H.H., and M.H. designed and generated *Prickle* mutant mice. A.P.M., T.P.Y., R.A., H. Sasaki, and A.S. provided various mice used in this study and analyzed the data. K.W. prepared recombinant Wnt5a protein and analyzed the corresponding data. T.F. and T.O. analyzed the data involving Celsr1 and Prickle2 antibodies, respectively. Y.O. determined precise localization of Vangl1 and Prickle2 proteins. D.S. performed quantitative analysis of Vangl1 protein localization. Y. Igarashi generated a program that automatically analyzes the position of the basal body in node cells. H.H. and K.M. wrote the paper.

SUPPLEMENTAL INFORMATION

Supplemental Information includes seven figures and one movie and can be found with this article online at http://dx.doi.org/10.1016/j.devcel.2017.02.010.

[10]Advanced Software Development Department, OLYMPUS Software Technology Corporation, 2-3 Kuboyama-cho, Hachioji-shi, Tokyo 192-8512, Japan

[11]Vertebrate Body Plan Group, RIKEN Center for Developmental Biology, 2-2-3 Minatojima-minamimachi, Chuo-ku, Kobe, Hyogo 650-0047, Japan

[12]Present address: National Institute of Genetics, Yata 1111, Mishima, Shizuoka 411-8540, Japan

[13]Present address: Max Planck Institute for Biophysical Chemistry, Am Fassberg 11, 37077 Gottingen, Germany

[14]Present address: Institute of Engineering, Tokyo University of Agriculture and Technology, Koganei, Tokyo 184-8588, Japan

[15]Present address: Centre for Organismal Studies, Heidelberg University, Heidelberg 69120, Germany

[16]Present address: Bristol-Myers Squibb, 6-5-1 Nishi-Shinjiku, Shinjiku, Tokyo 163-1328, Japan

[17]Present address: Faculty of Life Science, Kyoto Sangyo University, Kamigamo, Kita-ku, Kyoto 603-8555, Japan

[18]Lead Contact

SUMMARY

Polarization of node cells along the anterior-posterior axis of mouse embryos is responsible for left-right symmetry breaking. How node cells become polarized has remained unknown, however. *Wnt5a* and *Wnt5b* are expressed posteriorly relative to the node, whereas genes for Sfrp inhibitors of Wnt signaling are expressed anteriorly. Here we show that polarization of node cells is impaired in $Wnt5a^{-/-}$ $Wnt5b^{-/-}$ and *Sfrp* mutant embryos, and also in the presence of a uniform distribution of Wnt5a or Sfrp1, suggesting that Wnt5 and Sfrp proteins act as instructive signals in this process. The absence of planar cell polarity (PCP) core proteins Prickle1 and Prickle2 in individual cells or local forced expression of *Wnt5a* perturbed polarization of neighboring wild-type cells. Our results suggest that opposing gradients of Wnt5a and Wnt5b and of their Sfrp inhibitors, together with intercellular signaling via PCP proteins, polarize node cells along the anterior-posterior axis for breaking of left-right symmetry.

In Brief

Polarization of node cells along the anterior-posterior axis of mouse embryos is responsible for left-right symmetry breaking. Opposing gradients of Wnt5a and Wnt5b and of their Sfrp inhibitors, together with intercellular signaling via PCP proteins, polarize node cells along the anterior-posterior axis for breaking of left-right symmetry.

Graphical Abstract

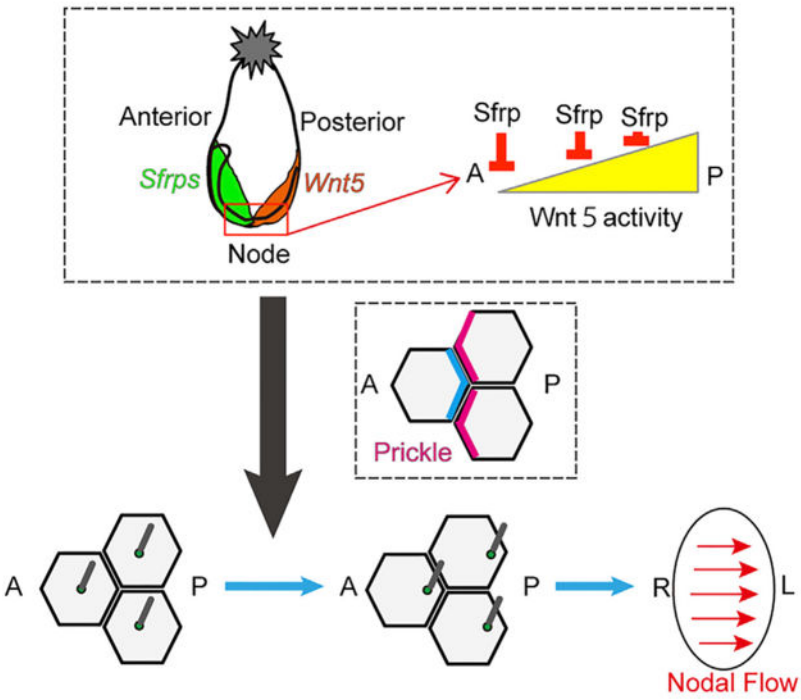

INTRODUCTION

Breaking of left-right (L-R) symmetry in vertebrates takes place at an early stage of embryogenesis in a region known as the ventral node (or equivalent structure) (Blum et al., 2008; Shiratori and Hamada, 2006). Cells at the ventral node each possess a motile cilium, the rotation of which generates a unidirectional fluid flow in the node cavity (Nonaka et al., 1998). In the mouse embryo, motile cilia at the node rotate in a clockwise direction, generating a leftward flow as a result of a posterior tilt of the rotational axis (Nonaka et al., 2005; Okada et al., 2005). Node cells are polarized along the anterior-posterior (A-P) axis by the planar cell polarity (PCP) mechanism, which regulates the coordinated polarization of cells in the plane of a tissue (Bayly and Axelrod, 2011; Goodrich and Strutt, 2011; Singh and Mlodzik, 2012), with PCP core proteins such as Disheveled (Dvl), Vangl1, and Prickle showing an anteriorly or posteriorly shifted localization in each node cell (Antic et al., 2010; Hashimoto et al., 2010; Song et al., 2010). Such polarized localization of PCP core proteins positions the basal body of the motile cilium to the posterior side of node cells, giving rise to the posterior tilt of the cilium. Positioning of centrioles is also regulated by Frizzled (Fz)-PCP signaling in *Drosophila* wings, suggesting that it is a conserved readout of PCP signaling (Carvajal-Gonzalez et al., 2016).

How the polarization of node cells is initiated has remained unknown. Pre-existing A-P positional information is presumably translated by node cells to give rise to the polarized localization of PCP core proteins, but the identity of such A-P information and the

mechanism of its translation are unclear. We have now examined the role of noncanonical Wnt signaling in node cell polarization in the mouse. Our results suggest that a combination of posteriorly shifted expression of Wnt5a and Wnt5b and anteriorly shifted expression of the Wnt antagonists Sfrps (secreted Frizzled-related proteins) generates asymmetry in Wnt5 activity with regard to the position of the node, and is responsible for polarization of node cells.

RESULTS

Role of Posteriorly Expressed Wnt5a and Wnt5b in Node Cell Polarization

We first examined whether Wnt proteins contribute to positioning of the basal body in node cells. Noncanonical Wnt signaling has recently been implicated in the establishment of PCP in various developmental contexts (Sokol, 2015), as exemplified by the role of Wnt11 in convergent extension during gastrulation (Heisenberg et al., 2000) as well as that of Wnt5a in inner ear formation (Qian et al., 2007) and limb patterning (Gao et al., 2011). At least three noncanonical Wnt genes—*Wnt5a*, *Wnt5b*, and *Wnt11*—are expressed near the node of the mouse embryo, and two of them (*Wnt5a* and *Wnt11*) are essential for axis elongation (Andre et al., 2015). Whereas *Wnt11* is expressed uniformly in and around the node (Figure S1), *Wnt5a* and *Wnt5b* are expressed asymmetrically with respect to the position of the node, being found preferentially on the posterior side (Figure 1A), an expression pattern that might be expected to generate an asymmetric distribution of Wnt activity along the A-P axis.

We examined node cells of *Wnt5a* and *Wnt5b* mutant mice for the average basal body position (ABP) (Hashimoto et al., 2010), which represents the relative position of the basal body within each cell along the A-P axis, with the anterior and posterior ends of a cell being defined as −1.0 and +1.0, respectively (Figure S2). The ABP of wild-type (WT) embryos is +0.3 (Hashimoto et al., 2010), reflecting the position of the basal body on the posterior side. The position of the basal body in $Wnt5a^{+/-}Wnt5b^{-/-}$ and $Wnt5a^{+/-}Wnt5b^{+/-}$ embryos was normal, with the ABP being indistinguishable from that of WT embryos. However, the ABP value was significantly reduced when both *Wnt5a* and *Wnt5b* were lost, with half (5/10) of $Wnt5a^{-/-}Wnt5b^{-/-}$ embryos showing an ABP below the control range (Figures 1B–1D), suggesting that the basal body failed to shift posteriorly in these embryos. Unidirectional laminar flow was also replaced with multiple vortical flows in half (2/4) of $Wnt5a^{-/-}Wnt5b^{-/-}$ embryos (Figures 2A–2E). Consistently, asymmetric *Nodal* expression was lost (1/5 embryos), downregulated (2/5 embryos), or normal (2/5 embryos) in $Wnt5a^{-/-}Wnt5b^{-/-}$ embryos (Figure 2K).

To determine whether Wnt ligands are also required for the polarized localization of PCP core proteins in node cells, we examined the localization of Vangl1, Vangl2, Prickle2, and Celsr1. By super-resolution imaging, Vangl1, Vangl2, and Prickle2 were found at the anterior side of node cells in WT embryos (Figures 3A–3F and S3; Movie S1). However, Vangl1 and Prickle2 were localized uniformly in $Wnt5a^{-/-}Wnt5b^{-/-}$ embryos (4/4 embryos for Vangl1) (Figures 3G–3I). Quantitative analysis of Vangl1 localization further supports that polarized localization of Vangl1 is impaired in $Wnt5a^{-/-}Wnt5b^{-/-}$ embryos (Figure 3H). Celsr1, which is found at the anterior and posterior sides of node cells in WT embryos, was also localized uniformly in $Wnt5a^{-/-}Wnt5b^{-/-}$ embryos (3/3 embryos) (Figure S3). These

findings suggested that Wnt5a and Wnt5b are required for correct basal body positioning and for the polarized localization of PCP core proteins in node cells.

Anteriorly Expressed Sfrps Are Also Essential for Node Cell Polarization

The position of the basal body was affected by the lack of both Wnt5a and Wnt5b, but this defect was apparent in only half of the mutant embryos. These results suggested the existence of additional genes that contribute to A-P asymmetric distribution of Wnt activity. Candidates for such genes included those for Sfrps, which contain a cysteine-rich domain (CRD) with homology to the Wnt binding domain of Frizzled and function as antagonists of Wnt-β-catenin and PCP pathways (Cruciat and Niehrs, 2013; Mii and Taira, 2011; Satoh et al., 2008). *Sfrp1*, *Sfrp2*, and *Sfrp5* are expressed in the developing mouse embryo (Matsuyama et al., 2009), with *Sfrp1* being expressed in the region anterior to the node—that is, on the side opposite to the expression domain of *Wnt5a* and *Wnt5b* (Figure 1A). *Sfrp2* and *Sfrp5* are also expressed preferentially in the region anterior to the node (Figure 1A). These expression patterns of *Sfrp* genes suggested that Sfrps may determine the level of Wnt5 activity in node cells.

To test this hypothesis, we examined the basal body position and the localization of PCP core proteins in node cells of Sfrp mutant embryos. The loss of these *Sfrps* had similar but more profound effects on node cell polarization compared with the lack of Wnt5a and Wnt5b. The position of the basal body was thus markedly altered in all (3/3) $Sfrp1^{-/-}Sfrp2^{-/-}Sfrp5^{-/-}$ embryos, and was also defective in many (6/8) of the $Sfrp1^{-/-}Sfrp2^{+/-}Sfrp5^{-/-}$ embryos examined (Figures 1B–1D). The PCP core proteins Vangl1, Vangl2, Prickle2, and Celsr1 were detected uniformly at the apical membrane of node cells, and thus failed to show a polarized localization, in the absence of Sfrp1, Sfrp2, and Sfrp5 (3/3 embryos for Vangl1) (Figures 3G–3J and S3). Consistent with these findings, nodal flow was severely impaired in all (3/3) $Sfrp1^{-/-}Sfrp2^{-/-}Sfrp5^{-/-}$ embryos, with the fluid flow consisting of both leftward and rightward elements but with rightward flow being dominant (Figures 2F–2H). Asymmetric *Nodal* expression was lost (1/3 embryos), downregulated on the left side (1/3 embryos), or reversed to the right side (1/3 embryos) in $Sfrp1^{-/-}Sfrp2^{-/-}Sfrp5^{-/-}$ embryos (Figure 2L). These results thus suggested that polarization of node cells along the A-P axis requires these three Sfrps.

Asymmetric Distribution of Wnt5 and Sfrp Proteins Is Required for Node Cell Polarization

The phenotype of the $Wnt5a^{-/-}Wnt5b^{-/-}$ and $Sfrp1^{-/-}Sfrp2^{-/-}\ Sfrp5^{-/-}$ embryos did not distinguish whether the corresponding proteins act as permissive or instructive signals for basal body positioning. To clarify this issue, we first examined whether a uniform distribution of Wnt5a impairs basal body positioning in node cells. We cultured WT embryos with recombinant Wnt5a from the late streak stage, when the basal body is localized in the central region of node cells (Hashimoto et al., 2010), and we then evaluated the posterior positioning of the basal body at the 3- to 5-somite stage. Compared with the control condition, treatment with recombinant Wnt5a (1 μg/mL) significantly reduced the ABP value (Figures 4A–4C), whereas the morphology of the node remained normal (Figure S1C). These results thus indicated that the uniform distribution of the exogenous Wnt5a protein affected the position of the basal body in node cells. Furthermore, the recombinant

Wnt5a did not rescue the basal body positioning defect of *Wnt5a*$^{-/-}$ *Wnt5b*$^{-/-}$ embryos (Figure 4C), suggesting that Wnt5 acts as an instructive signal not as a permissive factor. On the other hand, Wnt3a did not affect the basal body position in node cells at a concentration (0.8 μg/mL) that is known to induce Wnt signaling in the embryonic day 8 (E8.0) mouse embryo (Nakamura et al., 2012) (Figures 4D and S1D).

Culture of WT embryos with recombinant Sfrp1 (25 μg/mL) from the late streak stage also significantly reduced the ABP value (Figure 4E), suggesting that a uniform distribution of Sfrp1 protein impairs basal body positioning in node cells. The nonuniform distribution of Sfrps, rather than the presence of these proteins per se, thus also seems to be required for polarization of node cells.

We also induced *Wnt5a* expression in *Rosa*$^{Wnt5a/+}$ embryos with three different types of *Cre* transgene. Expression of *Wnt5a* was thus induced either uniformly with *Sox2-Cre* (Cha et al., 2014) or evenly around the node with *Noto-Cre*^{ERT2} (Ukita et al., 2009). The ABP value was reduced in about half (3/7) of the *Rosa*$^{Wnt5a/+}$;*Sox2-Cre* embryos examined (Figures 4F and S4A–S4C). More than half (3/5) of tamoxifen-treated *Rosa*$^{Wnt5a/+}$; *Noto-Cre*^{ERT2} embryos also showed a reduced ABP value (Figures 4G and S4D). These data suggested that uniform *Wnt5a* expression with respect to the node impairs the posterior positioning of the basal body, and thus provided further support for the importance of an asymmetric distribution of Wnt5 activity along the A-P axis for the polarization of node cells. Furthermore, forced *Wnt5a* expression with *Noto-Cre*^{ERT2} did not rescue the basal body positioning defect of *Wnt5a*$^{-/-}$ *Wnt5b*$^{-/-}$ mice (Figure 4G), again suggesting that Wnt5a acts instructively rather than permissively. Finally, we tested the effect of *Wnt5a* expression in the region anterior to the node with the use of an *Sfrp1-Cre*^{ERT2} transgene (Figure S4E). Again, the ABP value was reduced in most (4/6) tamoxifen-treated *Rosa*$^{Wnt5a/+}$;*Sfrp1-Cre*^{ERT2} embryos (Figure 4H).

Role of PCP Core Proteins Prickle1 and Prickle2 in Node Cell Polarization

Prickle1 (*Pk1*) and *Prickle2* (*Pk2*) are expressed in the ventral node (Figure S5A), and Pk2 protein shows a polarized localization at the anterior side of node cells (Antic et al., 2010) (Figure 3C). The function of Prickle proteins in the node has remained unknown, however. Deletion of *Pk1* in mice results in embryonic death due to defects in apicobasal polarity in the epiblast and subsequent gastrulation defects (Tao et al., 2009). To determine whether Prickle proteins play a role in the positioning of node cilia, we generated *Pk1* and *Pk2* mutant mice by deletion of exon 6 (Δex6) of each gene (Figures S5B and S5E). *Pk2*$^{Δex6/Δex6}$ mice showed no obvious developmental defects. In contrast to the embryonic mortality of the previously described *Pk1* null mice (Tao et al., 2009), *Pk1*$^{Δex6/Δex6}$ mice were born alive but died within 24 hr after birth, suggesting that the Δex6 allele of *Pk1* is hypomorphic. In *Pk1*$^{Δex6/Δex6}$ *Pk2*$^{Δex6/Δex6}$ embryos, nodal flow manifested multiple vortices (1/2 embryos; Figures 2I and 2J). Asymmetric *Nodal* expression was lost (1/3 embryos) or downregulated (2/3 embryos) in *Pk1*$^{Δex6/Δex6}$ *Pk2*$^{Δex6/Δex6}$ embryos (Figure 2M). The ABP value was reduced in all (4/4) *Pk1*$^{Δex6/Δex6}$ *Pk2*$^{Δex6/Δex6}$ embryos examined (Figures 5A–5C), indicating that the basal body failed to shift posteriorly in the absence of Prickle1 and Prickle2.

To clarify the relation between Prickle and Vangl1, we examined the localization of Vangl1 in node cells of *Pk1*$^{\Delta ex6/\Delta ex6}$*Pk2*$^{\Delta ex6/\Delta ex6}$ embryos. As described previously (Antic et al., 2010; Song et al., 2010), Vangl1 and Prickle2 are asymmetrically distributed at the anterior side of node cells in control embryos (Figures 3A, 3C, and 5D). In the node of *Pk1*$^{\Delta ex6/\Delta ex6}$*Pk2*$^{\Delta ex6/\Delta ex6}$ embryos, however, Vangl1 was detected uniformly around the cell-cell boundaries, although its apical localization was maintained (Figure 5D). Quantitative analysis of Vangl1 localization further supports that polarized localization of Vangl1 is impaired in *Pk1*$^{\Delta ex6/\Delta ex6}$*Pk2*$^{\Delta ex6/\Delta ex6}$ embryos (Figure 5E), indicating that Prickle1 and Prickle2 play a key role in the positioning of node cilia and are also required for the polarized localization of Vangl1 in node cells.

Role of Intercellular Communication via PCP Core Proteins in Basal Body Positioning

In *Drosophila*, interaction between PCP core proteins plays an essential role in the establishment of PCP (Bayly and Axelrod, 2011; Fanto and McNeill, 2004; Yang and Mlodzik, 2015). In mutant embryos such as *Wnt5a*$^{-/-}$*Wnt5b*$^{-/-}$ embryos in which the ABP value was found to be reduced, the node contained cells both with a normal and an abnormal basal body position. These two cell populations were not randomly distributed within the node but tended to form clusters (Figure S6), suggestive of an influence of cell-cell interaction. To examine the possible role of cell-cell interaction in basal body positioning, we generated chimeric embryos that contained both WT cells and *Pk1*$^{\Delta ex6/\Delta ex6}$*Pk2*$^{\Delta ex6/\Delta ex6}$ cells through aggregation of *Pk1*$^{\Delta ex6/\Delta ex6}$*Pk2*$^{\Delta ex6/\Delta ex6}$ embryos with WT embryonic stem cells (Figure 6A). In chimeric embryos with a relatively small contribution of WT cells, individual WT cells were often surrounded by mutant cells. Importantly, the basal body in such WT cells failed to become positioned at the posterior side (16/21 cells; Figures 6B–6E). Polarized Vangl1 localization was often impaired in WT cells surrounded by *Pk1*$^{\Delta ex6/\Delta ex6}$*Pk2*$^{\Delta ex6/\Delta ex6}$ cells (13/48 cells, Figure S7). This probably reflects the previous observations (Bastock et al., 2003) that Vangl protein physically interacts with PK proteins. In chimeric embryos with a higher contribution of WT cells, polarization of the WT cells was again impaired by neighboring *Pk1*$^{\Delta ex6/\Delta ex6}$*Pk2*$^{\Delta ex6/\Delta ex6}$ cells even if the WT cells were not completely surrounded by the mutant cells (Figures 6F–6H). These results thus suggested that the absence of Prickle proteins influences the polarization of neighboring WT cells in a non-cell-autonomous manner. This is unexpected, as Pk acts mostly cell-autonomously in the *Drosophila* wing (Tree et al., 2002). One possible difference is the way mosaics are generated in the two systems: coherent clones via mitotic divisions in *Drosophila* as opposed to chimeric mouse embryos where WT and mutant cells can mix.

Local Forced Expression of *Wnt5a* Impairs Polarization of Nearby Cells

Finally, we examined how locally enforced expression of *Wnt5a* in the node might influence polarization of nearby cells. Pregnant mice harboring *Rosa*$^{Wnt5a/+}$;*Noto-Cre*^{ERT2};*CAG-CAT-EGFP* embryos were administered a low dose of tamoxifen to induce *Wnt5a* expression in a subset of node cells. Subsequent examination of these embryos revealed two patterns of basal body localization. In the type I pattern (Figures 7A and 7E), node cells ectopically expressing *Wnt5a* (identified on the basis of EGFP expression) showed a centrally positioned basal body (41/58 cells), likely as a result of a uniform distribution of Wnt5a around these cells. The basal body of neighboring cells also remained in a central position

(48/69 cells), possibly as a result of impaired signaling via PCP core proteins between the *Wnt5a*-expressing cell and the neighboring cell. In the type II pattern (Figures 7B and 7E), the position of the basal body was normal in node cells showing ectopic *Wnt5a* expression (17/58 cells) but was affected in neighboring cells (14/34 cells). Interestingly, in some cases (3/17 type II cells), neighboring cells posterior to the *Wnt5a*-expressing cell showed anterior localization of the basal body. In the case of isolated *Wnt5a*-expressing cells, neighboring cells with an abnormally positioned basal body were apparent over a distance of at least two or three cells from the *Wnt5a*-expressing cell (Figures 7A and 7B), suggesting that local expression of *Wnt5a* can influence cell polarization over a distance of several cells. Vangl1 localization was similarly impaired by local forced *Wnt5a* expression. Thus, Vangl1 localization was defective not only in *Wnt5a*-expressing cells (Figure 7C, type I) (19/26 cells: Figure 7E) but also in neighboring cells of type I (22/39 cells) and those of type II (7/11 cells) *Wnt5a*-expressing cells (Figures 7D and 7E).

DISCUSSION

The role of PCP core proteins has been well established for PCP in *Drosophila*. On the other hand, little is known of the potential existence of a positional cue acting upstream of PCP core proteins as well as the possible role of Wnt ligands in PCP. In the wing epithelium of *Drosophila*, protocadherins (Fat and Dachsous) have been proposed to function as a long-range cue that acts upstream of PCP core proteins (Ma et al., 2003), raising the possibility that Wnt ligands do not contribute to PCP. On the other hand, observations in *Drosophila* (Wu et al., 2013) and vertebrates (Gros et al., 2009) have provided support for an instructive role of Wnt ligands in PCP (Yang and Mlodzik, 2015).

Our data now suggest that asymmetric activity of Wnt5a and Wnt5b serves as an upstream regulator of PCP core proteins in the polarization of mouse node cells. The opposite patterns of *Wnt5a/5b* and *Sfrp* gene expression observed along the A-P axis of the node would thus be expected to generate a graded distribution of Wnt5a/5b activity and might thereby provide a global cue for positioning of the basal body of the motile cilium at the posterior side of each node cell. Individual node cells may sense the differential level of Wnt5a/5b activity at their anterior and posterior sides, resulting in the initiation of asymmetric localization of PCP core proteins such as Prickle1, Prickle2, Vangl1, and Dvl at the anterior or posterior side of the cell. Interaction between PCP core proteins, both at the intracellular level (such as between Prickle and Dvl) and intercellular level (such as between Vangl1/2 and Fz or through Celsr1) would then establish robust A-P polarity in node cells (Figure 7F). In this regard, it is important to know expression and localization of Wnt receptors, in particular FZ proteins, in node cells.

The precise mechanisms of intracellular and intercellular signaling mediated by PCP core proteins in node cells remain unknown. However, previous observations in various experimental systems provide a basis for speculation about such mechanisms. Given that Prickle2 and Vangl1 are both expressed at the anterior side of node cells and physically associate with each other (Bastock et al., 2003; Jenny et al., 2003), the absence of one might be expected to alter the localization of the other within a cell, as we have now observed for the localization of Vangl1 in $Pk1^{\Delta ex6/\Delta ex6}Pk2^{\Delta ex6/\Delta ex6}$ embryos. Intercellular signaling via

PCP core proteins likely involves preferential association of such proteins in neighboring cells. The Frizzled-Dvl complex promotes enrichment of the Vangl2-Prickle complex across the cell junction with neighboring cells, which may account for the localization patterns of Prickle1/2, Vangl1, and Dvl in node cells. If this is the case, the absence of Prickle in a single cell would impair polarization not only of this cell but also of neighboring cells, as we have now observed with chimeric embryos consisting of both WT and $Pk1^{\Delta ex6/\Delta ex6}Pk2^{\Delta ex6/\Delta ex6}$ cells. Theoretically, the absence of Prickle1/2 in a single cell could have a long-range effect, but such an effect may be prevented by the presence of the Wnt5a/5b activity gradient.

Among the various mutant embryos examined in the present study, the defect in basal body positioning was most pronounced in the $Sfrp1^{-/-}Sfrp2^{-/-}Sfrp5^{-/-}$ embryos. Thus, whereas this defect was variable in $Wnt5a^{-/-}Wnt5b^{-/-}$ embryos, it was apparent with an ABP of about −0.1 in all $Sfrp1^{-/-}Sfrp2^{-/-}Sfrp5^{-/-}$ embryos examined. These results suggest that the anteriorly expressed Wnt inhibitors (Sfrps) play a more profound role in the generation of asymmetric Wnt activity than do the posteriorly expressed Wnt5a and Wnt5b. They thus further suggest that Wnt ligands other than Wnt5a and Wnt5b may contribute to basal body positioning, although our data suggest that such a role for Wnt11 is unlikely. All *Wnt* genes expressed near the node, including those expressed equally on both sides of the node, may contribute to Wnt activity around the node. The level of Wnt activity would be A < P in total, but this asymmetry would be much sharpened by the anteriorly expressed Sfrps.

The observed opposing gene expression patterns for Wnt5a/5b and their Sfrp inhibitors would be expected to generate an asymmetric distribution of Wnt activity with regard to the node. However, it is currently technically difficult to directly visualize noncanonical Wnt activity in an embryo. Also unclear is how a node cell would sense different levels of Wnt activity at its anterior and posterior ends. The noncanonical Wnt signaling pathway may play a role, but it is not clear which receptor is responsible. It has been suggested that in the *Drosophila* wing the asymmetric Wnt exposure will tether Fz proteins toward the Wnt source and hence initiate the PCP factor interactions with a directional bias (Wu et al., 2013). However, involvement of Fz proteins in node cell polarization remains to be investigated. Finally, the basal body is initially present at a central position of each node cell but then moves toward the posterior side during a period of several hours (Hashimoto et al., 2010). It remains unknown how the basal body changes its position by interpreting the localization of PCP core proteins. While actin is a key mediator that positions centrioles in *Drosophila* wings (Carvajal-Gonzalez et al., 2016), it is unknown whether a similar mechanism operates in mouse node cells. These questions will need to be answered in future studies to provide a full understanding of the mechanism of L-R symmetry breaking.

STAR★METHODS

CONTACT FOR REAGENT AND RESOURCE SHARING

Further information and requests for resources and reagents should be directed to and will be fulfilled by the Lead Contact, Hiroshi Hamada (hiroshi.hamada@riken.jp).

EXPERIMENTAL MODEL AND SUBJECT DETAILS

Mice—*Rosa*$^{Wnt5a/+}$ mice (Cha et al., 2014), *Sox2-Cre* mice (Hayashi et al., 2002), *Noto-Cre*^{ERT2} mice (Ukita et al., 2009), CAG-CAT-EGFP (Kawamoto et al., 2000) mice, as well as *Wnt5a* (Yamaguchi et al., 1999), *Wnt5b* (Agalliu et al., 2009), *Wnt11* (Majumdar et al., 2003), and *Sfrp1*, *Sfrp2*, and *Sfrp5* (Satoh et al., 2006, 2008) mutant mice were described previously. *Prickle1*$^{\Delta ex6/+}$ and *Prickle2*$^{\Delta ex6/+}$ mice were generated by conventional gene targeting in ES cells (Figure S5). Specific polymerase chain reaction (PCR) primers for detection of WT and mutant *Prickle* alleles included Pk1-WT-F (5'-AATCGGCGAATGCCAATG-3') and Pk1-WT- R (GGATTTCATCCCTAACACACCAC) for the *Prickle1*$^{+}$ allele; Pk1-Mut-F (GTGACTGCAAACAAGCGAAA) and Pk1-Mut-R (GCATTGACTTGCCACCAGTA) for the *Prickle1*$^{\Delta ex6}$ allele; Pk2-WT-F (CACATACATGCACACCCACAATTC) and Pk2-WT-R (TCAGGGTTGTTTTCAACTTCAAAGC) for the *Prickle2*$^{+}$ allele; and Pk2-WT-F and Pk2-Mut-R (GGCCTCTATGGAAGGGAAAG) for the *Prickle2*$^{\Delta ex6}$ allele. *Sfrp1-Cre*^{ERT2} mice were generated with the use of a mouse *Sfrp1* bacterial artificial chromosome (BAC) clone in which the first exon of *Sfrp1* is replaced by *Cre*^{ERT2}. All mouse experiments were approved by the relevant committees of Osaka University and RIKEN Center for Developmental Biology, license numbers FBS-12–019 and AH28–01.

METHOD DETAILS

Whole-Mount In Situ Hybridization and X-gal Staining—Whole-mount in situ hybridization was performed according to standard protocols with specific RNA probes for *Wnt5a*, *Wnt5b*, *Wnt11*, *Prickle1*, *Prickle2*, *Sfrp1*, *Sfrp2*, and *Sfrp5*. Expression of the *lacZ* transgene was detected by fixing transgenic embryos with paraformaldehyde and glutaraldehyde followed by staining transgenic embryos with X-gal (5-bromo-4-chloro-3-indoyl-β-D-galactoside) as described previously (Saijoh et al., 1999).

Immunostaining—Dissected embryos were fixed with 4% paraformaldehyde, dehydrated with methanol, and permeabilized with 0.1% Triton X-100 in phosphate-buffered saline. They were stained with primary antibodies and Alexa Fluor–conjugated secondary antibodies (invitrogen) by incubation overnight at 4°C. Primary antibodies included those to Zo-1 (mouse monoclonal, 1:10 dilution; kindly provided by S. Tsukita, Osaka University), to Vangl1 (rabbit polyclonal, 1:250 dilution; Sigma), Vangl2 (rabbit polyclonal, 1:250 dilution; Sigma), to Odf2 (rabbit polyclonal, 1:250 dilution; kindly provided by S. Tsukita or rabbit polyclonal, 1:250 dilution; Abcam), to Celsr1 (pig polyclonal, 1:100 dilution) (Shi et al., 2014), to EGFP (rat monoclonal, clone No. GF-090R, 1:100 dilution; Nacaai Tesque) and to Prickle2 (rabbit polyclonal, 1:100 dilution) (Hida et al., 2011). Fluorescence images were acquired with an FV-1000 confocal microscope (Olympus).

Super-Resolution Images—Two super-resolution methods were employed for the precise localization of PCP core proteins in node cells. In the first method, the sagittal sections (4 μm thick) were prepared from immunostained node samples and were observed by a Zeiss Elyra PS.1 system. Alternatively, the node regions of whole embryo were observed with a super-resolution microscopy based on the confocal microscope optics (Hayashi and Okada, 2015). Briefly, the raw images were taken with the objective lens,

HCPLAPO 40/1.10 W CORR CS2 on a SP-8 confocal microscope (Leica). The pinhole was reduced to the size corresponding 0.5 Airy unit at 580 nm. Three dimensional twice oversampled data were further processed by the classical maximum likelihood estimation deconvolution algorithm (Huygens, Scientific Volume Imaging) to enhance the high resolution components beyond the classical diffraction limit of 200 nm. Two-dimensional maps are shown by projection along the axis parallel to the apico-basal axis of the node pit cells. The three-dimensional (3D) views of the node were reconstructed from serial images (Z-stack) obtained by super-resolution imaging.

Whole-Embryo Culture and Recombinant Protein Treatment—Mouse embryos were dissected into phenol red–free Dulbecco's modified Eagle's medium (DMEM) supplemented with 10% fetal bovine serum (Invitrogen), transferred to a 50-ml tube containing DMEM supplemented with 75% rat serum (prepared by us), and cultured with rotation in an incubator containing 5% CO_2 at 37°C. The embryos were cultured in the presence of BSA (control) or recombinant proteins from the late streak stage to the three- to five-somite stage. The final concentrations of the recombinant proteins were 200 ng/ml for Wnt5a (Green et al., 2013; Willert, 2008), 1.0 μg/ml for Wnt5a (645-WN, R&D Systems), 0.8 μg/ml for Wnt3a (5036-WN, R&D Systems), and 25 μg/ml for Sfrp1 (5396-SF-025, R&D Systems).

Observation of Nodal Flow by PIV Analysis—Nodal flow was observed by multipoint scanning confocal microscopy and particle image velocimetry (PIV) analysis as described previously (Shinohara et al., 2012). Dissected embryos were first cultured under 5% CO_2 at 37°C in phenol red–free DMEM supplemented with 75% rat serum for ~30 min. The region containing the node was then excised, and the node cavity was filled with DMEM supplemented with 10% fetal bovine serum and fluorescent microbeads (0.2 μm in diameter) with excitation and emission wavelengths of 505 and 515 nm, respectively (Invitrogen). The motion of the beads was monitored in planes of +5 and +10 μm relative to the cavity for 10 s (30 frames per second) with the use of a CSU-X or CSU-W1 confocal unit (Yokogawa) and an iXon EMCCD camera (Andor Technology) connected to a DMI6000B microscope (Leica) equipped with a 63× glycerin-immersion objective lens. Time-series images for PIV analysis were captured at a resolution of 512 by 512 pixels and were processed with interrogation windows of 16 by 16 pixels with 50% overlap, corresponding to a spatial resolution of 4.3 by 4.3 μm. The time-averaged velocity distributions were calculated for 10-s intervals.

Quantitative Analysis of Basal Body Position—The average basal body position (ABP) represents the relative position of the basal body in each node cell along the A-P axis (vertical), as described previously (Hashimoto et al., 2010). Confocal images of the node immunostained for Odf2 and Zo-1 were obtained to determine the position of the basal body in each node cell (Figures S2A and S2B). For characterization of the shape and orientation of the node cells, the outline of each cell was calculated from the pattern of Zo-1 staining with the use of the ImageJ software plugin (http://rsb.info.nih.gov/nih-image/) to apply watershed segmentation (binary watershed line image in Figure S2C). The basal body was traced manually according to the Odf2 staining image, and the x,y coordinates of each basal

body were recorded using of the graphical user interface (GUI) in MATLAB software (Figure S2D). The relative value for the position of the basal body in each cell was calculated from the coordinate data with the anterior and posterior ends of a cell expressed as −−1.0 and +1.0, respectively (Figure S2E). This approach was programmed by one of the authors, Y. Igarashi. To examine if changes in cell morphology may influence ABP, we have examined cell morphology by quantitatively measuring the ratio of X/Y axis of each node cell (Figure S6). Although the ratio (morphology) varies among node cells, there is no significant difference between wild-type, *Wnt5a*$^{-/-}$ *Wnt5b*$^{-/-}$ and *Sfrp* triple mutant embryos, suggesting that changes in cell shape do not account for the reduced ABP in these mutant embryos.

Quantitative Analysis of PCP Core Protein Localization in Node Cells—The principle of the image analysis method for quantification of the polarity of staining signals within cell contours has been previously described (Aigouy et al., 2010; Shi et al., 2014). The cell boundary was traced manually from the pattern of Zo-1 staining and the x,y coordinates of each cellular contour were recorded. The Vangl1 staining intensities of the pixels in the contour were collected as $I(x, y)$. $I(x, y)$ was transformed into $I(r, \theta)$, where r is the distance between the pixel and the center of the cell while θ is the angle indicating the position of the pixel. Then, we calculated the average value of $I(r, \theta)$ for each θ section with a 5° range. The average value was set to $S(\theta_m)$, where θ_m is the center θ value of the section. The polarity of the staining signals φ ($-90° \leq \varphi < 90°$) was determined for each cell to fit: $\cos 2\varphi = Q_1/\sqrt{Q_1^2 + Q_2^2}$, $\sin 2\varphi = Q_2/\sqrt{Q_1^2 + Q_2^2}$ where $Q_1 = \Sigma\, S(\theta_m)\cos 2\theta_m$, $Q_2 = \Sigma\, S(\theta_m)\sin 2\theta_m$. Processing was performed in Excel. This approach was programmed by one of the authors, Dongbo Shi. Rose diagrams were drawn by using MATLAB.

Cre-Mediated Recombination—Expression of *Cre*^{ERT2} transgenes in embryos was induced by oral administration of tamoxifen (Sigma) in corn oil to pregnant mice either at a dose of 5 mg both 24 and 12 hr before the late streak stage (for the normal induction protocol) or at a dose of 1 mg 12 hr before the late streak stage (for suboptimal induction).

Generation of Chimeric Embryos—Mutant (*Pk1*$^{\Delta ex6/\Delta ex6}$ *Pk2*$^{\Delta ex6/\Delta ex6}$) embryos at the eight-cell stage were aggregated with wild-type ES cells expressing EGFP. The aggregated embryos at the blastocyst stage were transferred to the uterus of pseudopregnant mice and allowed to develop until E8.0. Embryos between the 3- and 5-somite stage were used for further analysis.

QUANTIFICATION AND STATISTICAL ANALYSIS

Statistical analysis was performed with Student's two-tailed *t* test, Wilcoxon rank-sum test or Watson's two-sample test of homogeneity by using R. A p value of <0.05 was considered statistically significant.

Supplementary Material

Refer to Web version on PubMed Central for supplementary material.

ACKNOWLEDGMENTS

We thank J. Miyazaki (Osaka University) for the CAG-CAT-EGFP mouse; K. Okamoto (University of Tokyo) for Software of particle image velocimetry analysis; A. Fukumoto for technical assistance; and K. Mizuno (RIKEN CDB) for his help in statistical analysis. This study was supported by grants from the Ministry of Education, Culture, Sports, Science, and Technology of Japan (nos. 24113001 and 24113004) and by Core Research for Evolutional Science and Technology of the Japan Science and Technology Corporation.

REFERENCES

Agalliu D, Takada S, Agalliu I, McMahon AP, and Jessell TM (2009). Motor neurons with axial muscle projections specified by Wnt4/5 signaling. Neuron 61, 708–720. [PubMed: 19285468]

Aigouy B, Farhadifar R, Staple DB, Sagner A, Roper JC, Julicher F, and Eaton S (2010). Cell flow reorients the axis of planar polarity in the wing epithelium of Drosophila. Cell 142, 773–786. [PubMed: 20813263]

Andre P, Song H, Kim W, Kispert A, and Yang Y (2015). Wnt5a and Wnt11 regulate mammalian anterior-posterior axis elongation. Development 142, 1516–1527. [PubMed: 25813538]

Antic D, Stubbs JL, Suyama K, Kintner C, Scott MP, and Axelrod JD (2010). Planar cell polarity enables posterior localization of nodal cilia and left-right axis determination during mouse and *Xenopus* embryogenesis. PLoS One 5, e8999. [PubMed: 20126399]

Bastock R, Strutt H, and Strutt D (2003). Strabismus is asymmetrically localised and binds to Prickle and Dishevelled during *Drosophila* planar polarity patterning. Development 130, 3007–3014. [PubMed: 12756182]

Bayly R, and Axelrod JD (2011). Pointing in the right direction: new developments in the field of planar cell polarity. Nat. Rev. Genet. 12, 385–391. [PubMed: 21502960]

Blum M, Weber T, Beyer T, and Vick P (2008). Evolution of leftward flow. Semin. Cell Dev. Biol. 20, 464–471. [PubMed: 19056505]

Carvajal-Gonzalez JM, Roman AC, and Mlodzik M (2016). Positioning of centrioles is a conserved readout of Frizzled planar cell polarity signalling. Nat. Commun. 7, 11135. [PubMed: 27021213]

Cha J, Bartos A, Park C, Sun X, Li Y, Cha SW, Ajima R, Ho HY, Yamaguchi TP, and Dey SK (2014). Appropriate crypt formation in the uterus for embryo homing and implantation requires Wnt5a-ROR signaling. Cell Rep. 8, 382–392. [PubMed: 25043182]

Cruciat CM, and Niehrs C (2013). Secreted and transmembrane wnt inhibitors and activators. Cold Spring Harbor Perspect. Biol 5, a015081.

Fanto M, and McNeill H (2004). Planar polarity from flies to vertebrates. J. Cell Sci. 117, 527–533. [PubMed: 14730010]

Gao B, Song H, Bishop K, Elliot G, Garrett L, English MA, Andre P, Robinson J, Sood R, Minami Y, et al. (2011). Wnt signaling gradients establish planar cell polarity by inducing Vangl2 phosphorylation through Ror2. Dev. Cell 20, 163–176. [PubMed: 21316585]

Goodrich LV, and Strutt D (2011). Principles of planar polarity in animal development. Development 138, 1877–1892. [PubMed: 21521735]

Green JL, Bauer M, Yum KW, Li YC, Cox ML, Willert K, and Wahl GM (2013). Use of a molecular genetic platform technology to produce human Wnt proteins reveals distinct local and distal signaling abilities. PLoS One 8, e58395. [PubMed: 23516471]

Gros J, Serralbo O, and Marcelle C (2009). WNT11 acts as a directional cue to organize the elongation of early muscle fibres. Nature 457, 589–593. [PubMed: 18987628]

Hashimoto M, Shinohara K, Wang J, Ikeuchi S, Yoshiba S, Meno C, Nonaka S, Takada S, Hatta K, Wynshaw-Boris A, et al. (2010). Planar polarization of node cells determines the rotational axis of node cilia. Nat. Cell Biol. 12, 170–176. [PubMed: 20098415]

Hayashi S, and Okada Y (2015). Ultrafast superresolution fluorescence imaging with spinning disk confocal microscope optics. Mol. Biol. Cell 26, 1743–1751. [PubMed: 25717185]

Hayashi S, Lewis P, Pevny L, and McMahon AP (2002). Efficient gene modulation in mouse epiblast using a Sox2Cre transgenic mouse strain. Gene Expr. Patterns 2, 93–97. [PubMed: 12617844]

Heisenberg CP, Tada M, Rauch GJ, Saude L, Concha ML, Geisler R, Stemple DL, Smith JC, and Wilson SW (2000). Silberblick/Wnt11 mediates convergent extension movements during zebrafish gastrulation. Nature 405, 76–81. [PubMed: 10811221]

Hida Y, Fukaya M, Hagiwara A, Deguchi-Tawarada M, Yoshioka T, Kitajima I, Inoue E, Watanabe M, and Ohtsuka T (2011). Prickle2 is localized in the postsynaptic density and interacts with PSD-95 and NMDA receptors in the brain. J. Biochem. 149, 693–700. [PubMed: 21324980]

Jenny A, Darken RS, Wilson PA, and Mlodzik M (2003). Prickle and Strabismus form a functional complex to generate a correct axis during planar cell polarity signaling. EMBO J. 22, 4409–4420. [PubMed: 12941693]

Kawamoto S, Niwa H, Tashiro F, Sano S, Kondoh G, Takeda J, Tabayashi K, and Miyazaki J (2000). A novel reporter mouse strain that expresses enhanced green fluorescent protein upon Cre-mediated recombination. FEBS Lett. 470, 263–268. [PubMed: 10745079]

Ma D, Yang CH, McNeill H, Simon MA, and Axelrod JD (2003). Fidelity in planar cell polarity signalling. Nature 421, 543–547. [PubMed: 12540853]

Majumdar A, Vainio S, Kispert A, McMahon J, and McMahon AP (2003). Wnt11 and Ret/Gdnf pathways cooperate in regulating ureteric branching during metanephric kidney development. Development 130, 3175–3185. [PubMed: 12783789]

Matsuyama M, Aizawa S, and Shimono A (2009). Sfrp controls apicobasal polarity and oriented cell division in developing gut epithelium. PLoS Genet. 5, e1000427. [PubMed: 19300477]

Mii Y, and Taira M (2011). Secreted Wnt “inhibitors” are not just inhibitors: regulation of extracellular Wnt by secreted Frizzled-related proteins. Dev. Growth Differ. 53, 911–923. [PubMed: 21995331]

Nakamura T, Saito D, Kawasumi A, Shinohara K, Asai Y, Takaoka K, Dong F, Takamatsu A, Belo JA, Mochizuki A, et al. (2012). Fluid flow and interlinked feedback loops establish left-right asymmetric decay of Cerl2 mRNA. Nat. Commun. 3, 1322. [PubMed: 23271656]

Nonaka S, Tanaka Y, Okada Y, Takeda S, Harada A, Kanai Y, Kido M, and Hirokawa N (1998). Randomization of left-right asymmetry due to loss of nodal cilia generating leftward flow of extraembryonic fluid in mice lacking KIF3B motor protein. Cell 95, 829–837. [PubMed: 9865700]

Nonaka S, Yoshiba S, Watanabe D, Ikeuchi S, Goto T, Marshall WF, and Hamada H (2005). De novo formation of left-right asymmetry by posterior tilt of nodal cilia. PLoS Biol. 3, e268. [PubMed: 16035921]

Okada Y, Takeda S, Tanaka Y, Izpisua Belmonte JC, and Hirokawa N (2005). Mechanism of nodal flow: a conserved symmetry breaking event in left-right axis determination. Cell 121, 633–644. [PubMed: 15907475]

Qian D, Jones C, Rzadzinska A, Mark S, Zhang X, Steel KP, Dai X, and Chen P (2007). Wnt5a functions in planar cell polarity regulation in mice. Dev. Biol. 306, 121–133. [PubMed: 17433286]

Saijoh Y, Adachi H, Mochida K, Ohishi S, Hirao A, and Hamada H (1999). Distinct transcriptional regulatory mechanisms underlie left-right asymmetric expression of lefty-1 and lefty-2. Genes Dev. 13, 259–269. [PubMed: 9990851]

Satoh W, Gotoh T, Tsunematsu Y, Aizawa S, and Shimono A (2006). Sfrp1 and Sfrp2 regulate anteroposterior axis elongation and somite segmentation during mouse embryogenesis. Development 133, 989–999. [PubMed: 16467359]

Satoh W, Matsuyama M, Takemura H, Aizawa S, and Shimono A (2008). Sfrp1, Sfrp2, and Sfrp5 regulate the Wnt/beta-catenin and the planar cell polarity pathways during early trunk formation in mouse. Genesis 46, 92–103. [PubMed: 18257070]

Shi D, Komatsu K, Hirao M, Toyooka Y, Koyama H, Tissir F, Goffinet AM, Uemura T, and Fujimori T (2014). Celsr1 is required for the generation of polarity at multiple levels of the mouse oviduct. Development 141, 4558–4568. [PubMed: 25406397]

Shinohara K, Kawasumi A, Takamatsu A, Yoshiba S, Botilde Y, Motoyama N, Reith W, Durand B, Shiratori H, and Hamada H (2012). Two rotating cilia in the node cavity are sufficient to break left-right symmetry in the mouse embryo. Nat. Commun. 3, 622. [PubMed: 22233632]

Shiratori H, and Hamada H (2006). The left-right axis in the mouse: from origin to morphology. Development 133, 2095–2104. [PubMed: 16672339]

Singh J, and Mlodzik M (2012). Planar cell polarity signaling: coordination of cellular orientation across tissues. Wiley Interdiscip. Rev. Dev. Biol. 1, 479–499. [PubMed: 23066429]

Sokol SY (2015). Spatial and temporal aspects of Wnt signaling and planar cell polarity during vertebrate embryonic development. Semin. Cell Dev. Biol. 42, 78–85. [PubMed: 25986055]

Song H, Hu J, Chen W, Elliott G, Andre P, Gao B, and Yang Y (2010). Planar cell polarity breaks bilateral symmetry by controlling ciliary positioning. Nature 466, 378–382. [PubMed: 20562861]

Tao H, Suzuki M, Kiyonari H, Abe T, Sasaoka T, and Ueno N (2009). Mouse prickle1, the homolog of a PCP gene, is essential for epiblast apical-basal polarity. Proc. Natl. Acad. Sci. USA 106, 14426–14431. [PubMed: 19706528]

Tree DR, Shulman JM, Rousset R, Scott MP, Gubb D, and Axelrod JD (2002). Prickle mediates feedback amplification to generate asymmetric planar cell polarity signaling. Cell 109, 371–381. [PubMed: 12015986]

Ukita K, Hirahara S, Oshima N, Imuta Y, Yoshimoto A, Jang CW, Oginuma M, Saga Y, Behringer RR, Kondoh H, et al. (2009). Wnt signaling maintains the notochord fate for progenitor cells and supports the posterior extension of the notochord. Mech. Dev. 126, 791–803. [PubMed: 19720144]

Willert KH (2008). Isolation and application of bioactive Wnt proteins. Methods Mol. Biol. 468, 17–29. [PubMed: 19099243]

Wu J, Roman AC, Carvajal-Gonzalez JM, and Mlodzik M (2013). Wg and Wnt4 provide long-range directional input to planar cell polarity orientation in *Drosophila*. Nat. Cell Biol. 15, 1045–1055. [PubMed: 23912125]

Yamaguchi TP, Bradley A, McMahon AP, and Jones S (1999). A Wnt5a pathway underlies outgrowth of multiple structures in the vertebrate embryo. Development 126, 1211–1223. [PubMed: 10021340]

Yang Y, and Mlodzik M (2015). Wnt-Frizzled/planar cell polarity signaling: cellular orientation by facing the wind (Wnt). Annu. Rev. Cell Dev. Biol 31, 623–646. [PubMed: 26566118]

Highlights

- A gradient of Wnt5 activity polarizes node cells along the A-P axis
- A Wnt5 activity asymmetry induces polarized localization of PCP proteins
- Prickle proteins play a non-cell-autonomous role acting downstream of Wnt5a asymmetry

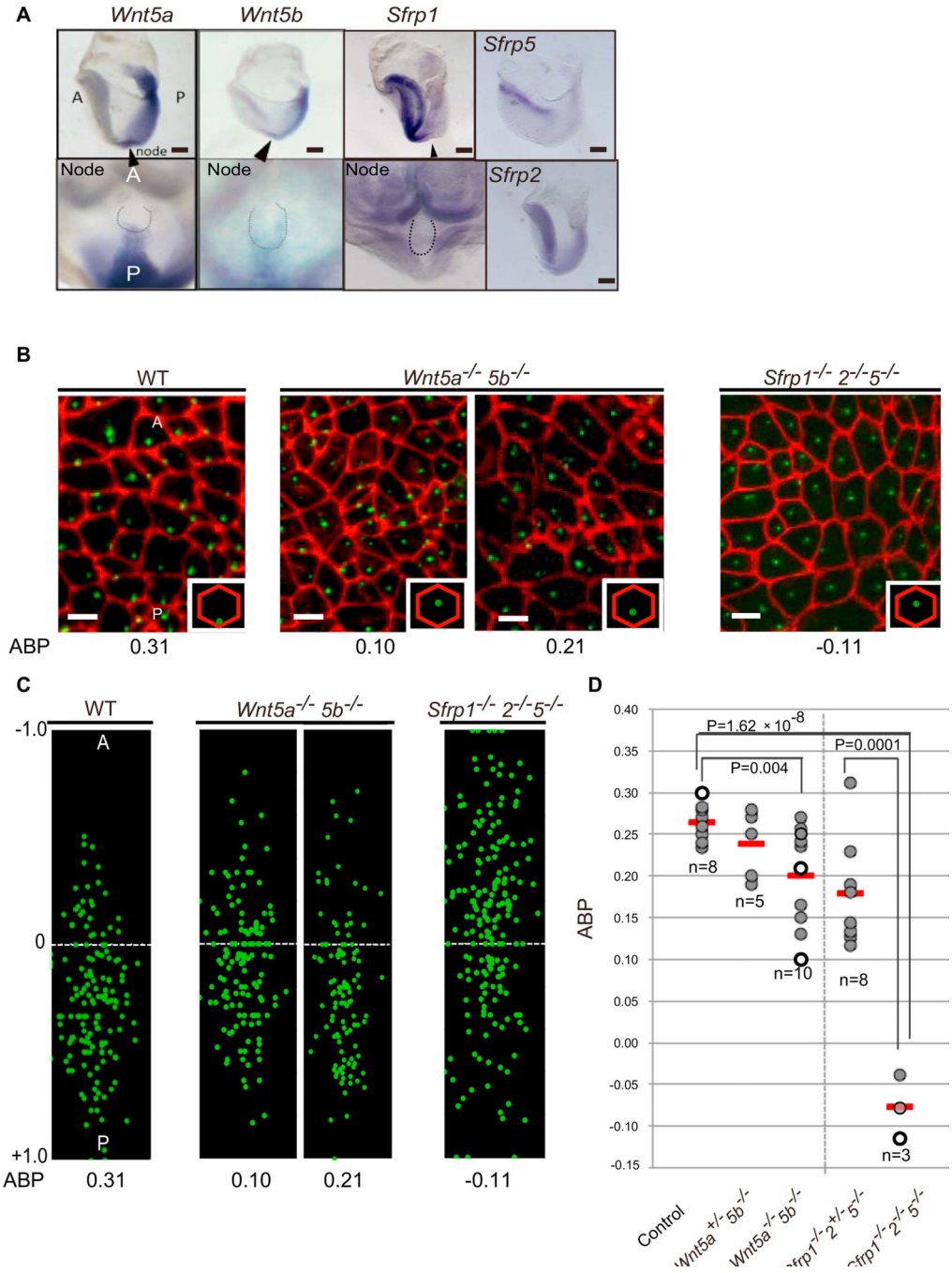

Figure 1. *Wnt5* and *Sfrp* Genes that Show Opposite Expression Patterns Are Required for Correct Positioning of the Basal Body in Node Cells

(A) Whole-mount in situ hybridization analysis of *Wnt5a*, *Wnt5b*, and *Sfrp* gene expression in mouse embryos at embryonic day 7.5 (E7.5). Arrowheads indicate the position of the node, which is shown outlined in the corresponding lower images. Scale bars, 100 μm.

(B) Immunofluorescence staining for the tight junction protein Zo-1 (red) and the basal body protein Odf2 (green) in mouse embryos of the indicated genotypes at the 3- to 5-somite stage. Only the node regions are shown. Whereas the basal body (green) is located at the posterior side of node cells in the WT embryo, it is located centrally in those of *Wnt5a*

$^{-/-}$ *Wnt5b*$^{-/-}$ and *Sfrp1*$^{-/-}$ *Sfrp2*$^{-/-}$ *Sfrp5*$^{-/-}$ embryos. Two types of *Wnt5a*$^{-/-}$ *Wnt5b*$^{-/-}$ embryos, showing severe (ABP = 0.10) and less severe (ABP = 0.21) defects, are shown. Schematic representations of the Odf2 and Zo-1 staining patterns are shown in the insets. Scale bars, 5 μm.

(C) Relative position of the basal body in node cells of mouse embryos of the indicated genotypes at the 3- to 5-somite stage. Each green dot corresponds to a single node cell. The ABP of each embryo is also shown.

(D) Summary of ABP values for embryos of the indicated genotypes. Control embryos include *Wnt5a*$^{+/-}$, *Wnt5b*$^{+/-}$, *Wnt5b*$^{-/-}$, and *Wnt5a*$^{+/-}$ *Wnt5b*$^{+/-}$ genotypes. Each point denotes the ABP of a single embryo. Open circles correspond to the embryos shown in (B). The red bars indicate mean values. The p values for the indicated comparisons were determined with Student's two-tailed t test.

A, anterior; P, posterior. See also Figures S1 and S2.

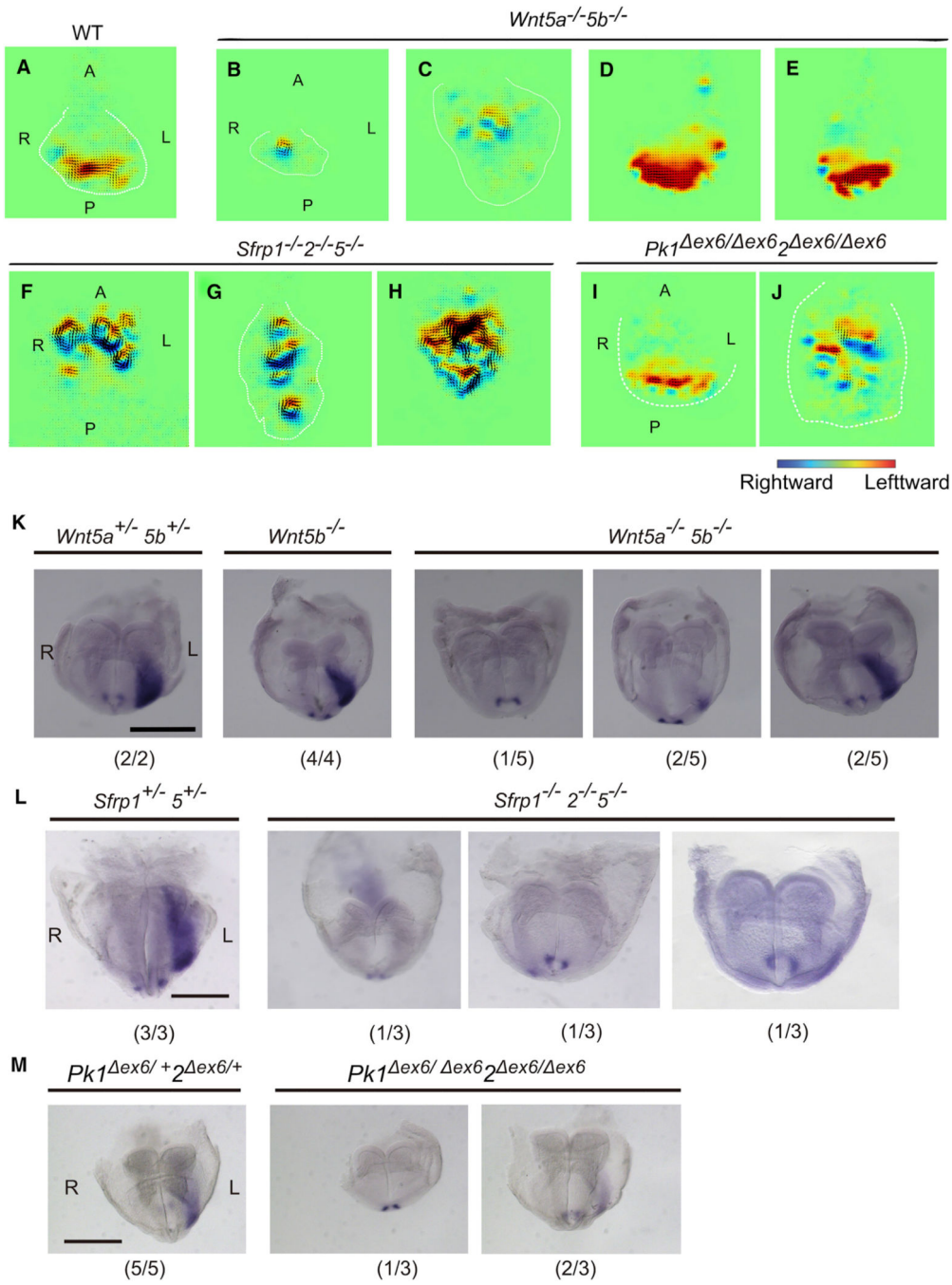

Figure 2. Nodal Flow and *Nodal* Expression Are Impaired in *Wnt5*, *Sfrp* and *Prickle* Mutant Mice

(A–J) Nodal flow was examined in wild-type (WT) (A), *Wnt5a*$^{-/-}$ *Wnt5b*$^{-/-}$ (B–E), *Sfrp1*$^{-/-}$ *Sfrp2*$^{-/-}$ *Sfrp5*$^{-/-}$ (F–H), and *Prickle1*$^{\Delta ex6/\Delta ex6}$ *Prickle2*$^{\Delta ex6/\Delta ex6}$ (I and J) mouse embryos at the 3- to 5-somite stage by particle image velocimetry (PIV) analysis with fluorescent microbeads. The white line indicates the outline of the node. Small arrows indicate the direction and velocity of the flow at the indicated positions. The relative color scale indicates the magnitude of the flow velocity (leftward in red and rightward in blue).

Note that the leftward flow was detected in embryos shown in (A), (D), (E), and (I) but was lost in the remaining embryos.

(K–M) *Nodal* expression in the lateral plate, which is left-sided in WT embryo, was examined for mutant embryos with the indicated genotype at the 5- to 6-somite stage. The frequency of the embryo exhibiting each expression pattern is shown in parentheses. In $Wnt5a^{-/-}Wnt5b^{-/-}$ embryos (K), *Nodal* expression was lost (1/5 embryos), downregulated (2/5 embryos), or normal (2/5 embryos). In $Sfrp1^{-/-}Sfrp2^{-/-}Sfrp5^{-/-}$ embryos examined (L), *Nodal* expression was lost (1/3 embryos), weak Nodal expression was found on the right side (1/3 embryos) or weak expression was detected on the left side (1/3 embryos). In $Pk1^{\Delta ex6/\Delta ex6}Pk2^{\Delta ex6/\Delta ex6}$ embryos (M), left-sided *Nodal* expression was lost (1/3 embryos) or downregulated (2/3 embryos). Scale bar, 500 μm.

A, anterior; P, posterior; R, right; L, left.

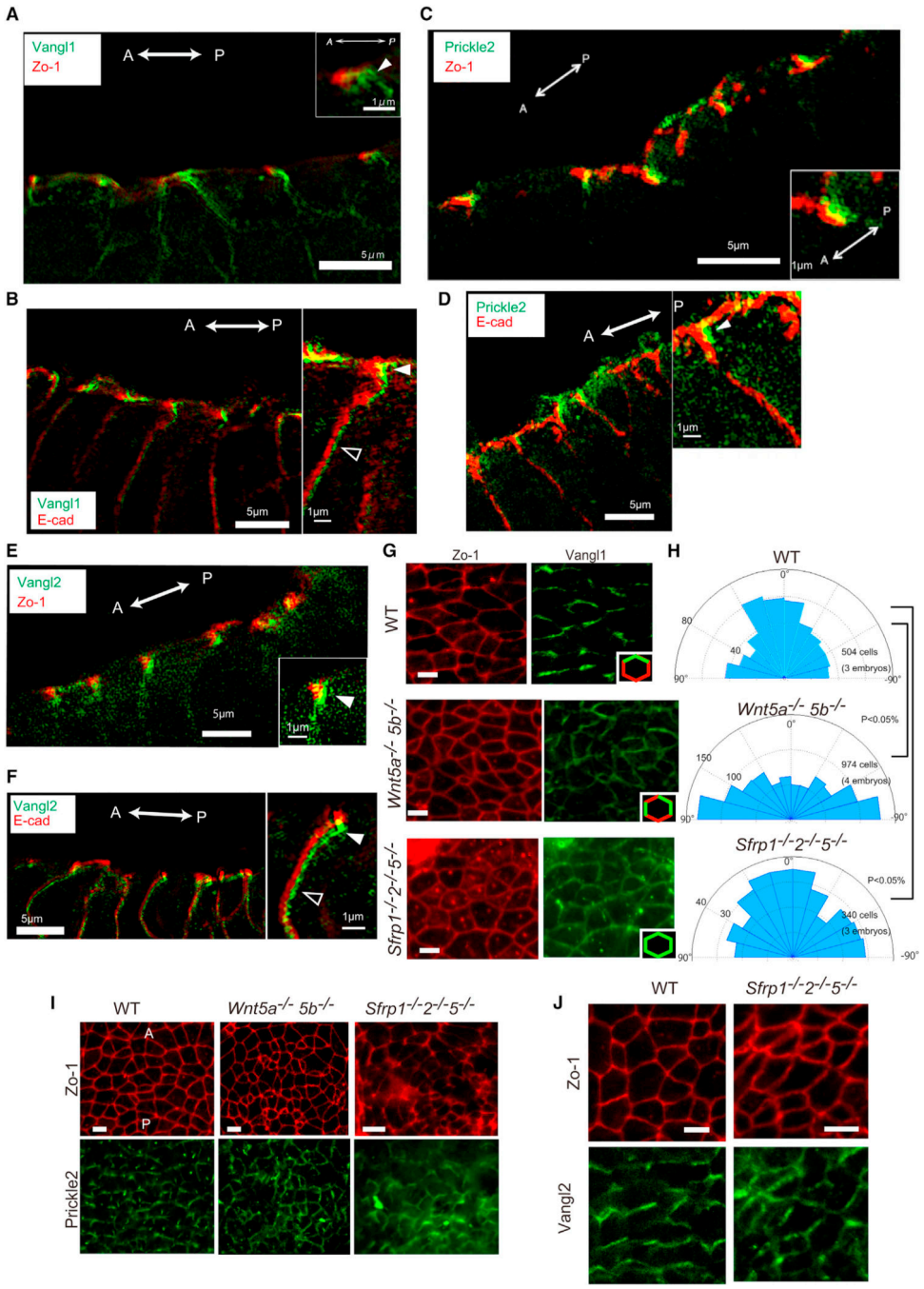

Figure 3. Polarized Localization of PCP Core Proteins Is Dependent on *Wnt5* and *Sfrp* Genes

(A–F) The subcellular localization of Vangl1, Prickle2, and Vangl2 in node cells of the WT embryo. Sagittal sections of the node stained for Vangl1 and Zo-1 (A), Vangl1 and E-cadherin (B), Prickle2 and Zo-1 (C), Prickle2 and E-cadherin (D), Vangl2 and Zo-1 (E), or Vangl2 and E-cadherin (F) were observed by super-resolution imaging. A higher-magnification image is also shown in each panel. White arrowheads indicate localization of these proteins to the anterior edge of the node cells. Vangl1, Prickle2, and Vangl2 proteins are apparently localized to the anterior side and apical side of node cells. Note that Vangl1

and Vangl2 show anterior localization even in the nonapical regions (open arrowheads in B and F).

(G) Localization of Zo-1 and Vangl1 in the node of WT, *Wnt5a*$^{-/-}$ *Wnt5b*$^{-/-}$, and *Sfrp1*$^{-/-}$ *Sfrp2*$^{-/-}$ *Sfrp5*$^{-/-}$ embryos at the 3- to 5-somite stage. The localization of Vangl1 in node cells is illustrated schematically in the insets in (G).

(H) Quantitative analysis of the Vangl1 localization pattern in individual embryos of the indicated genotypes. The angle (−90° to +90°) is determined by using quantitative analysis for each cell. In the rose diagram, angles are classed into 12 classes (15° for each class). The area size of each class indicates the cell numbers for each WT, *Wnt5a*$^{-/-}$ *Wnt5b*$^{-/-}$, and *Sfrp1*$^{-/-}$ *Sfrp2*$^{-/-}$ *Sfrp5*$^{-/-}$ embryos. The p values for the indicated comparisons were determined with Watson's two-sample test of homogeneity. The number of cells analyzed is 504 from three embryos (WT), 974 from four embryos (*Wnt5a*$^{-/-}$ *Wnt5b*$^{-/-}$), and 340 from three embryos (*Sfrp1*$^{-/-}$ *Sfrp2*$^{-/-}$ *Sfrp5*$^{-/-}$).

(I) Localization of Zo-1 (red) and Prickle2 (green) in the node of WT, *Wnt5a*$^{-/-}$ *Wnt5b*$^{-/-}$, and *Sfrp1*$^{-/-}$ *Sfrp2*$^{-/-}$ *Sfrp5*$^{-/-}$ embryos at the 3- to 5-somite stage.

(J) Localization of Zo-1 (red) and Vangl2 (green) in the node of WT and *Sfrp1*$^{-/-}$ *Sfrp2*$^{-/-}$ *Sfrp5*$^{-/-}$ embryos at the 3- to 5-somite stage. Note that the polarized localization of Vangl1 and Prickle2 is defective in the *Wnt5* and *Sfrp* mutant embryos. Vangl2 localization is also impaired in the *Sfrp* mutant embryo. Scale bars for (G)–(J), 5 μm. A, anterior; P, posterior. See also Figure S3.

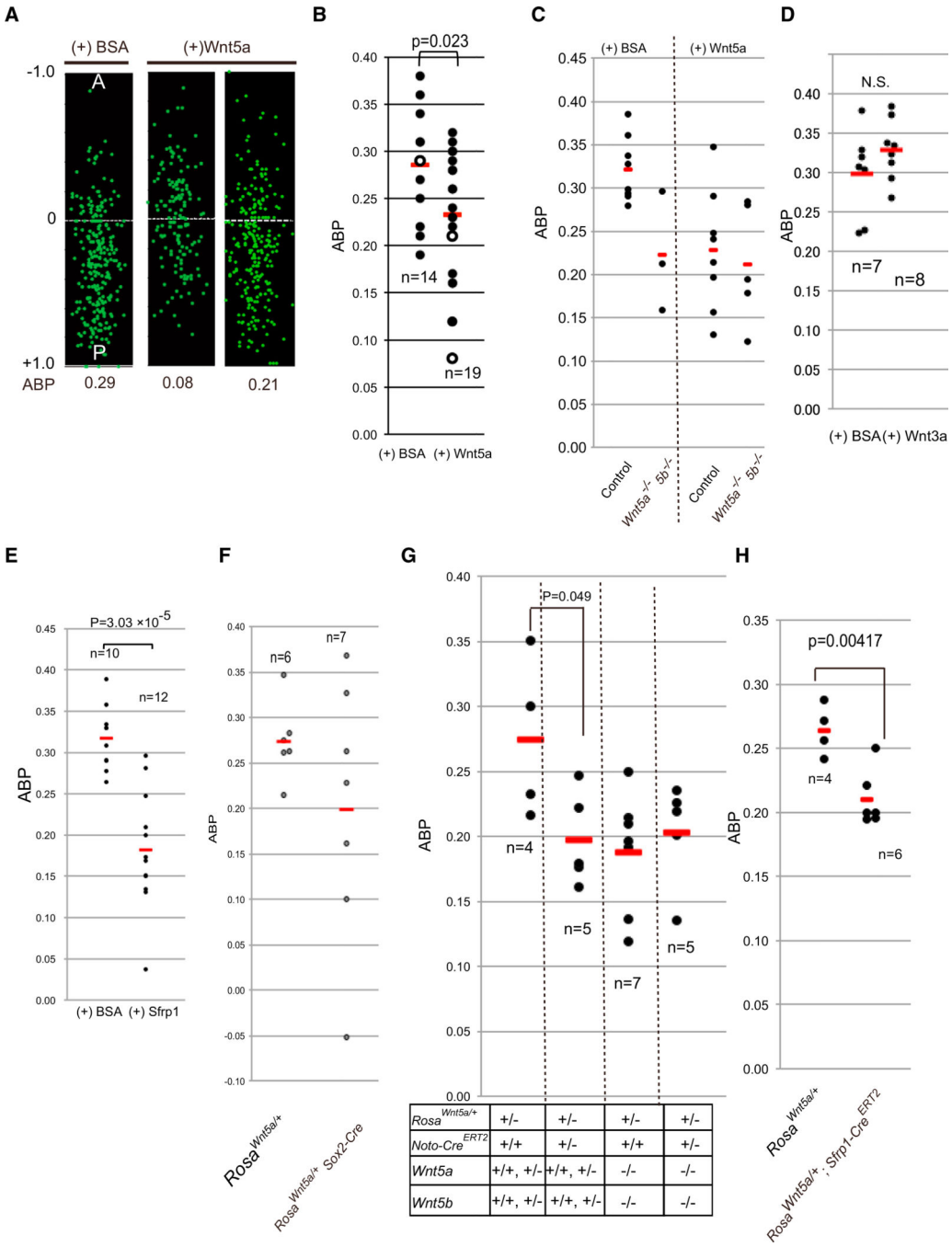

Figure 4. Perturbation of the Asymmetric Distribution of Wnt5a and Sfrp1 Impairs Node Cell Polarization

(A and B) WT embryos were cultured with BSA or recombinant Wnt5a (1 μg/mL) from the late streak stage to the 3- to 5-somite stage. The relative position of the basal body (green dots in A) of node cells was then determined. Two different embryos, showing defective ABP and less defective ABP, are shown for Wnt3a-treated embryos. Data are shown for representative embryos in (A) and are summarized for the indicated numbers of embryos in (B) (red bars indicate mean values). Three open dots in (B) correspond to three embryos shown in (A). A, anterior; P, posterior.

(C) ABP values for *Wnt5a*$^{-/-}$ *Wnt5b*$^{-/-}$ embryos cultured with BSA or recombinant Wnt5a as in (A). Control embryos include *Wnt5a*$^{+/-}$, *Wnt5b*$^{+/-}$, *Wnt5b*$^{-/-}$, and *Wnt5a*$^{+/-}$ *Wnt5b*$^{+/-}$ genotypes.

(D) ABP values for WT embryos cultured with BSA or recombinant Wnr3a (0.8 μg/mL) from the late streak to 3- to 5-somite stages. Note that Wnt3a did not affect the basal body position in node cells.

(E) ABP values for WT embryos cultured with BSA or recombinant Sfrp1 (25 μg/mL) from the late streak to 3- to 5-somite stages.

(F) ABP values for *Rosa*$^{Wnt5a/+}$ and *Rosa*$^{Wnt5a/+}$;*Sox2-Cre* embryos, in the latter of which *Wnt5a* expression is induced uniformly.

(G) ABP values for tamoxifen-treated *Rosa*$^{Wnt5a/+}$;*Noto-Cre*^{ERT2} and *Wnt5a*$^{-/-}$;*Wnt5b*$^{-/-}$;*Rosa*$^{Wnt5a/+}$;*Noto-Cre*^{ERT2} embryos, in which *Wnt5a* expression is induced evenly around the node.

(H) ABP values for tamoxifen-treated *Rosa*$^{Wnt5a/+}$;*Sfrp1-Cre*^{ERT2} embryos, in which *Wnt5a* expression is induced in the region anterior to the node.

Dams were treated orally with tamoxifen (5 mg) both 24 and 12 hr before the late streak stage for embryos in (G) and (H). The p values for the indicated comparisons were determined with Student's two-tailed t test. N.S., not significant. See also Figure S4.

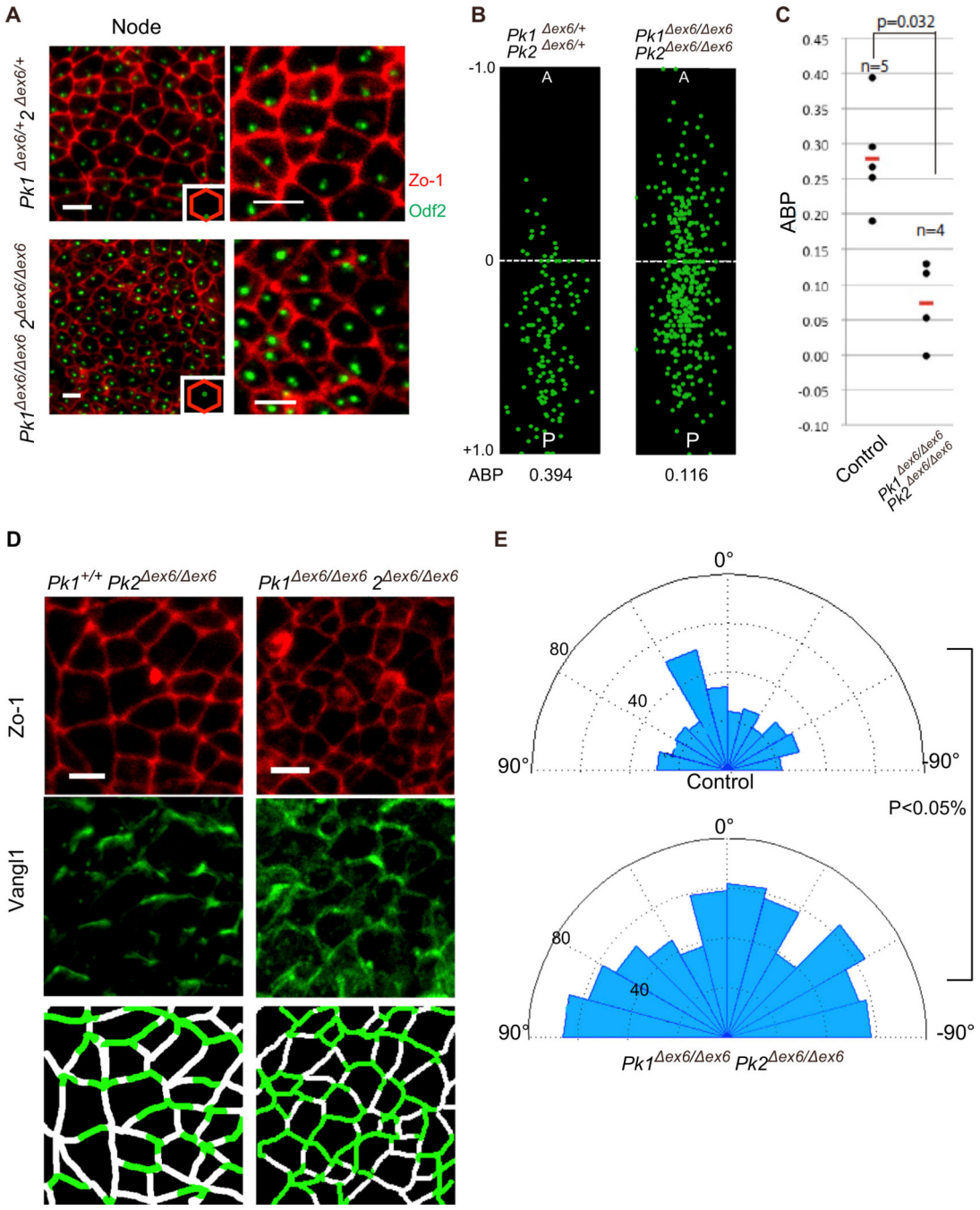

Figure 5. Polarization of Node Cells Requires Prickle 1 and Prickle 2

(A) Immunostaining of the node region of *Pk1*$^{\Delta ex6/+}$*Pk2*$^{\Delta ex6/+}$ (control) and *Pk1*$^{\Delta ex6/\Delta ex6}$*Pk2*$^{\Delta ex6/\Delta ex6}$ mouse embryos at the 3- to 5-somite stage for Zo-1 (red) and Odf2 (green). A, anterior; P, posterior.

(B) Relative position of the basal body (green dots) summarized for individual node cells of embryos as in (A). A, anterior; P posterior.

(C) ABP values for the indicated numbers of embryos as in (A). Red bars indicate mean values. Control embryos include *Pk1*$^{\Delta ex6/+}$*Pk2*$^{\Delta ex6/+}$ and *Pk2*$^{\Delta ex6/+}$genotypes.

(D) Immunostaining of *Pk2*$^{\Delta ex6/+}$ and *Pk1*$^{\Delta ex6/\Delta ex6}$*Pk2*$^{\Delta ex6/\Delta ex6}$ embryos at the 3- to 5-somite stage for Zo-1 (red) and Vangl1 (green). Note that the polarized localization of Vangl1 is impaired in the latter embryo. The Vangl1 localization pattern is schematically illustrated below (shown in green).

(E) Quantitative analysis of the Vangl1 localization pattern in the Control (*Pk2*$^{\Delta ex6/+}$ and *Pk1*$^{\Delta ex6/\Delta ex6}$*Pk2*$^{\Delta ex6/\Delta ex6}$) and *Pk1*$^{\Delta ex6/\Delta ex6}$*Pk2*$^{\Delta ex6/\Delta ex6}$ embryos. The angle (−90° to +90°) is determined by using quantitative analysis for each cell. In the rose diagram, angles are classed into 12 classes (15° for each class). The area size of each class indicates the cell numbers for Control and *Pk1*$^{\Delta ex6/\Delta ex6}$*Pk2*$^{\Delta ex6/\Delta ex6}$ embryos. The numbers of cells analyzed were 337 cells from three embryos for control and 654 cells from three embryos for *Pk1*$^{\Delta ex6/\Delta ex6}$*Pk2*$^{\Delta ex6/\Delta ex6}$.

The p values were determined with Watson's two-sample test of homogeneity. Scale bars, 5 μm. See also Figure S5.

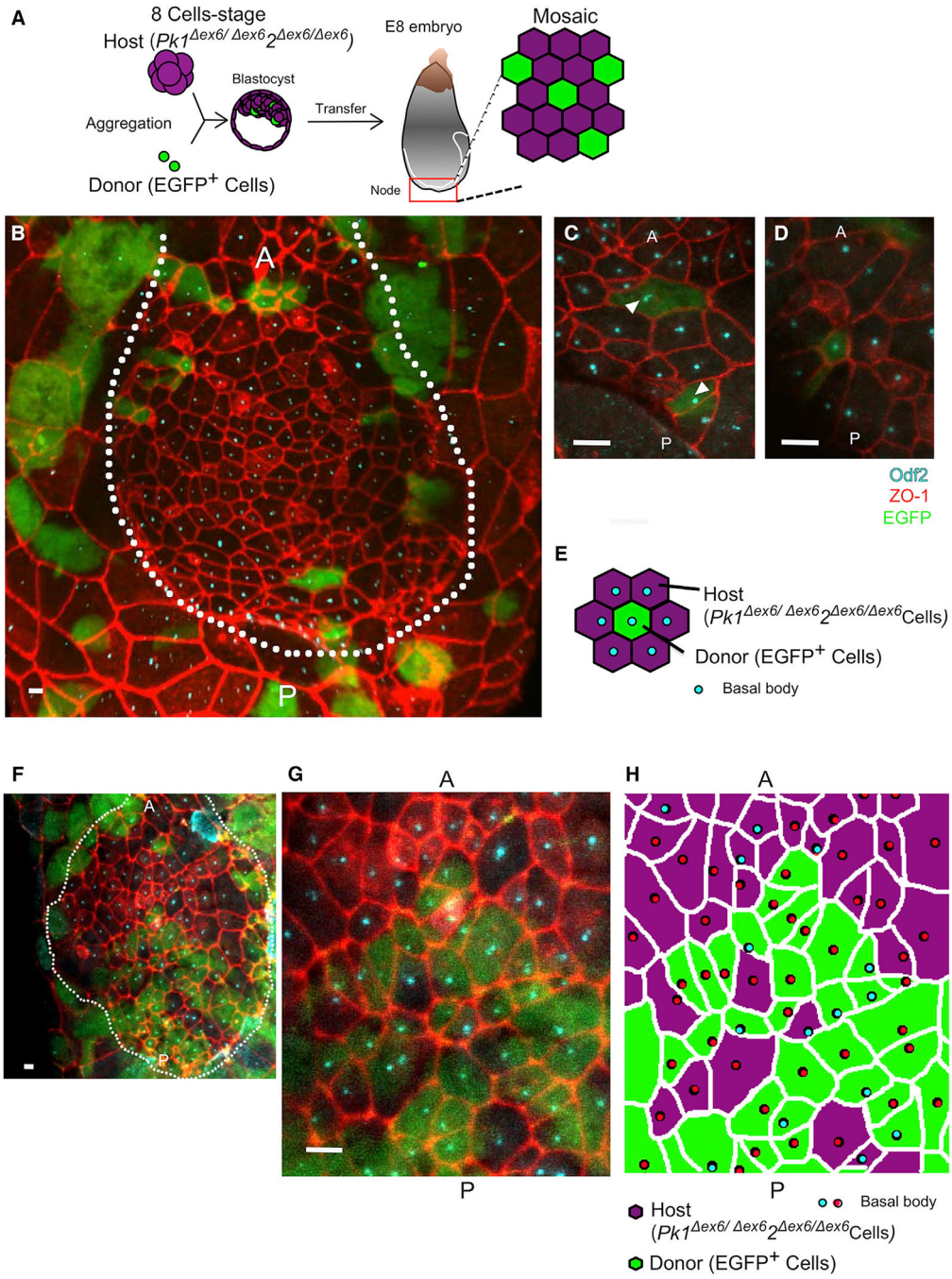

Figure 6. The Absence of Prickle 1 and Prickle 2 in Node Cells Affects the Polarization of Nearby WT Cells

(A) Experimental design for the generation of chimeric embryos consisting of both WT and *Pk1*$^{\Delta ex6/\Delta ex6}$*Pk2*$^{\Delta ex6/\Delta ex6}$ cells by aggregation of *Pk1*$^{\Delta ex6/\Delta ex6}$*Pk2*$^{\Delta ex6/\Delta ex6}$ embryos (host) with *Pk1*$^{+/+}$*Pk2*$^{+/+}$ embryonic stem cells (donor) that express EGFP.

(B–H) E8 chimeric embryos generated as in (A) with a low (B–E) or high (F–H) contribution of WT cells were immunostained for Zo-1 (red), Odf2 (light blue), and EGFP (green). The node regions are shown in (B) and (F), with higher-magnification images presented in (C), (D), and (G). Arrowheads in (C) indicate the basal body of the donor cell.

Schematic representations of basal body position in WT (EGFP-positive) and *Pk1*$^{\Delta ex6/\Delta ex6}$*Pk2*$^{\Delta ex6/\Delta ex6}$ cells of corresponding chimeric embryos are shown in (E) and (H). In (H), posteriorly located and centrally located centrioles are shown in blue and red, respectively. Note that the basal body in WT cells failed to become positioned at the posterior side when the WT cells were surrounded by *Pk1*$^{\Delta ex6/\Delta ex6}$*Pk2*$^{\Delta ex6/\Delta ex6}$ cells. A, anterior; P posterior. Scale bars, 5 μm. See also Figures S6 and S7.

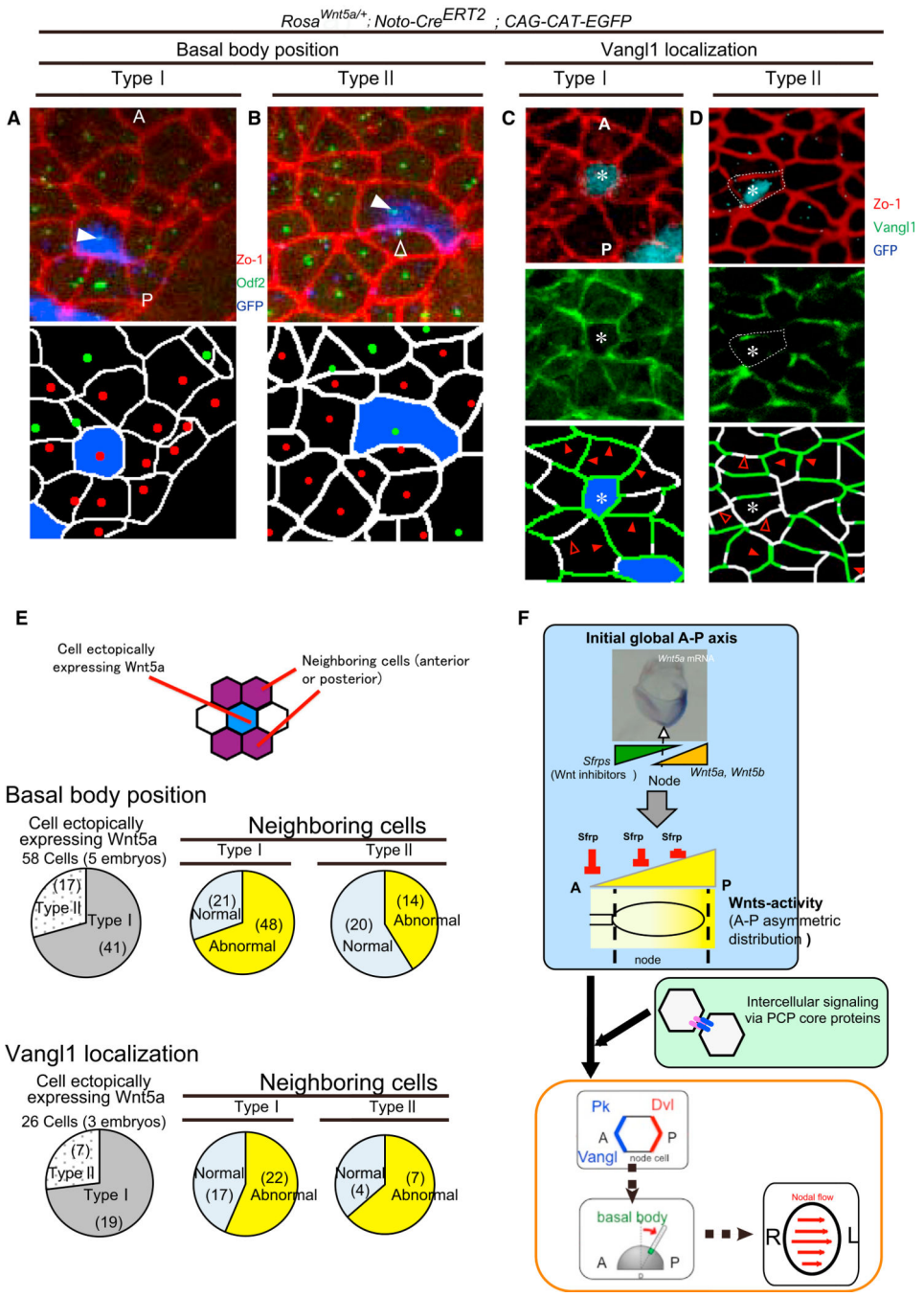

Figure 7. Local Forced Expression of *Wnt5a* Impairs Polarization of Nearby Node Cells

(A–D) Pregnant mice harboring *Rosa*$^{Wnt5a/+}$;*Noto-Cre*^{ERT2};*CAG-CAT-EGFP* embryos were treated with a low dose (1 mg) of tamoxifen at 12 hr before the late streak stage to induce *Wnt5a* expression in a subset of node cells. Embryos were recovered at the 3- to 5-somite stage and were immunostained for Zo-1 (red), Odf2 (green), and EGFP (blue) (A and B) or for Zo-1 (red), Vangl1 (green), and EGFP (light blue) (C and D). Node cells expressing *Wnt5a* were identified on the basis of EGFP expression. In (A) and (B), the position of the basal body in node cells is schematically illustrated below. Posteriorly located and centrally/

anteriorly located centrioles are shown in green and red, respectively. The majority of node cells expressing *Wnt5a* (type I, 41/58 cells) showed a centrally localized basal body (A, closed arrowhead), while the remaining cells (type II, 17/58 cells) showed posteriorly localized basal body (B, arrowhead). In both cases, the position of the basal body was defective in nearby cells (red dots in A and B). In some of the cells located posterior to the type II *Wnt5a*-expressing cell, the basal body was positioned at the anterior side (B, open arrowhead). In (C) and (D), the Vangl1 localization pattern in node cells is illustrated schematically below (shown in green). Red arrowheads denote the regions showing abnormal Vangl1 localization. The shape of the *Wnt5*-expressing cell in (D) is indicated by the dotted line. The majority of node cells expressing *Wnt5a* (type I, 19/26 cells) showed defective Vangl1 localization (C, asterisk), while the remaining cells (type II, 7/26 cells) showed normal Vangl1 localization (D, asterisk). In both cases, Vangl1 localization was defective in nearby cells (C and D, arrowheads; 22/39 cells for type I, 7/11 cells for type II).
(E) An illustration of *Wnt5a*-expressing and neighboring cells in *Rosa*$^{Wnt5a/+}$;*Noto-Cre*^{ERT2};*CAG-CAT-EGFP* embryos treated with a low dose (1 mg) of tamoxifen is shown on the top. Note that neighboring cells in this analysis are those located anteriorly or posteriorly to an *Wnt5a*-expressing cell. In the middle row, the numbers of type I and type II node cells are summarized for the *Rosa*$^{Wnt5a/+}$;*Noto-Cre*^{ERT2};*CAG-CAT-EGFP* embryos that were examined for the basal body position. Forty-one type I cells and 17 type II cells were detected in five such embryos. For type I and type II cells, the number of neighboring cells showing abnormal or normal Vangl1 localization is indicated (for example, among 69 neighboring cells adjacent to type I cells, 48 cells showed abnormal basal body position). In the bottom row, the numbers of type I and type II node cells are summarized for the *Rosa*$^{Wnt5a/+}$;*Noto-Cre*^{ERT2};*CAG-CAT-EGFP* embryos that were examined for Vangl1 localization. These numbers are expressed similarly: for example, among 39 neighboring cells adjacent to type I cells, 22 cells showed abnormal Vangl1 localization.
(F) Model for polarization of node cells based on asymmetric and opposing distributions of Wnt5a/5b and their Sfrp inhibitors together with intercellular signaling via PCP core proteins. Pk, Prickle.
A, anterior; P posterior. See Discussion for further details. See also Figures S6 and S7.

KEY RESOURCES TABLE

REAGENT or RESOURCE	SOURCE	IDENTIFIER
Antibodies		
Mouse monoclonal anti-Zo-1	S. Tsukita, Osaka University	N/A
Rabbit polyclonal anti-Vangl1	Sigma	HPA025235; RRID: AB_1858718
Rabbit polyclonal anti-Vangl2	Sigma	HPA027043; RRID: AB_10601709
Rabbit polyclonal anti-Odf2	S. Tsukita, Osaka University	N/A
Rabbit polyclonal anti-Odf2	Abcam	ab43840
Pig polyclonal Celsr1	T. Fujimori, Division of Embryology, National Institute for Basic Biology	Shi et al., 2014
Rat monoclonal ant- EGFP	Nacalai Tesque	No. GF-090R
Rabbit polyclonal Panti-rickle2	T. Ohtsuka, Yamanashi University	Hida et al., 2011
Chemicals, Peptides, and Recombinant Proteins		
Recombinant Human/Mouse Wnt-5a Protein	R&D	645-WN
Recombinant Human Wnt-3a Protein	R&D	5036-WN
Recombinant Human sFRP-1 Protein	R&D	5396-SF-025
Experimental Models: Cell Lines		
Wild-type ES cells expressing EGFP	M.Okabe, Osaka University	Act GFP ES
Experimental Models: Organisms/Strains		
Mouse: *Rosa*$^{Wnt5a/+}$	Terry P. Yamaguchi	Cha et al., 2014
Mouse: *Sox2-Cre*	Hayashi et al., 2002	N/A
Mouse:*Noto-Cre*^{ERT2}	Ukita et al., 2009	RBRC05283
Mouse:CAG-CAT-EGFP	Kawamoto et al., 2000	N/A
Mouse: *Wnt5a* mutant	Yamaguchi et al., 1999	N/A
Mouse: *Wnt5b* mutant	Agalliu et al., 2009	N/A
Mouse:*Sfrp1*, *Sfrp2*, and *Sfrp5* mutant	Satoh et al., 2006; Satoh et al., 2008	N/A
Mouse: *Prickle1*$^{\Delta ex6/+}$	This paper	RBRC06546
Mouse: *Prickle2*$^{\Delta ex6/+}$	This paper	RBRC06548
Mouse:*Sfrp1- Cre*^{ERT2} mice	This paper	N/A
Oligonucleotides		
Pk1-WT-F (5'-AATCGGCGAATGCCAATG-3') for the *Prickle1*$^{+}$ allele	This paper	N/A
Pk1-WT- R (GGATTTCATCCCTAACACACCAC) for the *Prickle1*$^{+}$ allele	This paper	N/A
Pk1-Mut-F (GTGACTGCAAACAAGCGAAA) for the *Prickle1*$^{\Delta ex6}$ allele	This paper	N/A
Pk1-Mut-R (GCATTGACTTGCCACCAGTA) for the *Prickle1*$^{\Delta ex6}$ allele	This paper	N/A
Pk2-WT-F (CACATACATGCACACCCACAATTC) for the *Prickle2*$^{+}$ allele and the *Prickle2*$^{\Delta ex6}$ allele	This paper	N/A

REAGENT or RESOURCE	SOURCE	IDENTIFIER
Pk2-WT-R (TCAGGGTTGTTTTCAACTTCAAAGC) for the *Prickle2*$^{+}$ allele	This paper	N/A
Pk2-Mut-R (GGCCTCTATGGAAGGGAAAG) for the *Prickle2*$^{\Delta ex6}$ allele	This paper	N/A
Recombinant DNA		
Sfrp1 bacterial artificial chromosome (BAC) clone	BAC PAC Resources Center	Clone:PR23-131J19
Software and Algorithms		
MATLAB R2012a	MathWorks	N/A
ImageJ software	Rasband, W.S., ImageJ, U. S. National Institutes of Health, Bethesda, Maryland, USA	http://rsb.info.nih.gov/nih-image/
Particle image velocimetry (PIV) analysis	This paper and Koji Okamoto (University of Tokyo)	N/A
Other		
Confocal scanner unit CSU-X1	Yokogawa	N/A
Confocal scanner unit CSU-W1	Yokogawa	N/A
iXon EMCCD camera	Andor Technology	N/A
DMI6000B microscope	Leica	N/A
FV-1000 confocal microscope	Olympus	N/A
Fluorescent microbeads (diameter of 0.2 μ m with excitation and emission wavelengths of 505 and 515 nm, respectively)	Invitrogen	F8811